

Ordering and phonons in $\text{Ba}_3\text{CaNb}_2\text{O}_9$ complex perovskite

João Elias Figueiredo Soares Rodrigues^a, Edvan Moreira^b, Débora Moraes Bezerra^c, Adeilton Pereira Maciel^c, Carlos William de Araujo Paschoal^{a,e,*}

^a*Departamento de Física, CCET, Universidade Federal do Maranhão, 65085-580, São Luís - MA, Brazil*

^b*Universidade Federal Rural do Semi-Árido, UFERSA, Campus Caraúbas, 59780-000, Caraúbas - RN, Brazil*

^c*Departamento de Química, CCET, Universidade Federal do Maranhão, 65085-580, São Luís - MA, Brazil*

^d*Departamento de Física, Universidade Federal do Ceará, Campus do Pici, 60455-760, Fortaleza - CE, Brazil*

^e*Department of Materials Science and Engineering, University of California Berkeley, 94720-1760, Berkeley - CA, United States*

Abstract

In this work we performed a detailed investigation about ordering in $\text{Ba}_3\text{CaNb}_2\text{O}_9$ perovskite. The sintering temperature and time were changed to obtain samples with different ordering. The order parameters were probed by Raman spectroscopy based on a partial disordered model. To use the partial disordered model correctly we performed *ab initio* calculations in $\text{Ba}_3\text{CaNb}_2\text{O}_9$ to assign the optical phonons. The results showed that sintering temperature improves order while sintering time is not so efficient to promote order.

Keywords: A. ceramics; A. oxides; B. chemical synthesis; C. Raman spectroscopy; D. crystal structure

PACS: 81.20.Ka, 81.05.Je, 78.30.Am, 61.05.cf

*Corresponding author: Phone: +55 98 3301 8222; Fax: +55 98 3301 8204; alternative e-mails: paschoal.william@gmail.com; paschoal.william@berkeley.edu

Email address: paschoal@ufma.br (Carlos William de Araujo Paschoal)

1. Introduction

Complex triple perovskites with the general formula $A_3B'B''O_9$, where A is an alkaline earth metal, B' and B'' are ions with valencies 2+ and 5+, have recently attracted much interest as high-temperature proton conductors [1, 2, 3, 4, 5, 6, 7] and as dielectric resonators [8, 9, 10, 11, 12, 13, 14]. Particularly, the nonstoichiometric series $Ba_3Ca_{1+x}Nb_{2x}O_{(9-3x)/2}$ has been extensively investigated due to its high proton conductivity and chemical stability [1, 4, 5, 6, 7]. In such oxides, the formation of oxygen vacancies is achieved by increasing the B'/B'' ratio. The vacancies can be filled with OH species upon annealing samples in water vapour at high temperatures and even OH^- concentration is small, the ionic conductivity can be dominated by proton transport [15], enabling it for application in fuel cells.

Despite oxygen vacancies can be highly mobile in simple ABO_3 perovskites,[16] in complex perovskites as $Ba_3CaNb_2O_9$ the vacancy mobility tends to be strongly influenced by the B'/B'' ratio, valencies and ordering. Substitutions in A and B sites of ABX_3 perovskites are responsible for improving a large part of the applications of these materials, bringing new physical and chemical properties.[8] However, the substitution by more than one ion, mainly in B site, can lead to structures which are disordered or ordered, according the new ions distribution into the structure. This substitution leads to new crystalline structures when there is a ordered distribution. B-site cation-ordered triple perovskites whose chemical formula is $A_3B'B''O_9$ are a particular family obtained by B-site substitution .

From the structural viewpoint, in the triple B-site ordered substitution (sometimes called 1:2 order), two main structures can be formed. In the First, an ordered B'/B'' substitution into B site can lead to a trigonal structure which belongs to the space group $P\bar{3}m1$. In this structure the cations B' and B'' are alternately distributed in $\{111\}$ planes in the form $\cdots B'B''B''B'B'B''B''B' \cdots$. Another possible structure for this composition is the so-called hexagonal $6H$ structure that belongs to the $P6_3/mmc$ space group, in which the $B'O_6$ and $B''O_6$ octahedra share edges.[7, 12]

However, partial disordered B'/B'' distribution in both structure can occur, with part of the B' cations occupying the B'' cation sites and vice versa. Partial disorder in perovskites plays an essential role because they strongly influence their physical properties. For example, order influences phonons and dielectric constant, implying in consequences for applications of 1:2 perovskites in wireless communication system.[17, 18, 19, 20, 21, 22, 11, 9, 23]

Disorder is particularly interesting in $\text{Ba}_3\text{CaNb}_2\text{O}_9$ perovskites because it favors a higher conductivity in these protonic conductors based on nonstoichiometry Ba compounds, which always have higher conductivity and lower activation energy than the corresponding Sr compounds.[2] Due to the importance of ordering in $\text{Ba}_3\text{CaNb}_2\text{O}_9$ (BCN) ceramics, mainly because its conductivity properties, in this work we proposed a systematically investigation of the order achievement in BCN complex perovskite.

2. Experimental Procedures

BCN samples were synthesized by polymeric precursor method using barium nitrate ($\text{Ba}(\text{NO}_3)_2$, Sigma Aldrich), calcium citrate tetrahydrate ($\text{Ca}_3(\text{C}_6\text{H}_5\text{O}_7)_2 \cdot 4\text{H}_2\text{O}$, Ecibra) and ammonium complex of niobium ($\text{NH}_4(\text{NbO}(\text{C}_2\text{O}_4)_2(\text{H}_2\text{O})_2) \cdot 3\text{H}_2\text{O}$, CBMM) as sources of metals [24]. Barium polymeric precursor was obtained by mixing aqueous solutions of barium nitrate and citric acid ($\text{C}_6\text{H}_8\text{O}_7 \cdot \text{H}_2\text{O}$, Proquímico) in a molar ratio of 1:3 metal-citric acid, keeping stirring between 60 and 70 °C . Finally, ethylene glycol ($\text{HOCH}_2\text{CH}_2\text{OH}$, Merck) was added to metal/Citric aqueous solution in a mass ratio of 1:1 in relation to citric acid. Calcium polymeric precursor was obtained following the same procedure for barium. To obtain niobium precursor we firstly precipitated niobium oxo-hydroxide stirring an aqueous solution of ammonium complex of niobium until pH of 9 in a thermal bath at 0 °C . Niobium hydroxide ($\text{Nb}(\text{OH})_5$) was separated from oxalate ions using distilled water at 40-50 °C under vacuum filtering. Finally, citric acid and ethylene glycol were added to the Niobium hydroxide aqueous solution. The pH of the polymeric precursors was kept at the same values to avoid precipitations when mixing them. To determine the necessary precursor weight to achieve the correct metal stoichiometry to form BCN perovskite we used gravimetric analysis at 900 °C for 1 h. We mixed the three precursors and heated the mixture between 80 and 90 °C to form the polyester resin, which had high viscosity and glassy. The resin was annealed at 400 °C for 2h. This heat treatment converted the resin in a black porous powder. This powder was lightly grounded using an agate mortar. After it was calcined at 1300 °C for 2h to obtain BCN sample. This sample is our reference to investigate the ordering process and it will be referenced as *start sample* along this work. From this reference sample, several pellets were sintered at different temperatures and time of sintering to investigate the ordering phenomena.

The crystalline structure of the samples were probed by powder X-ray

diffraction (XRD - Bruker D8 Advance). We performed a continuous scanning mode using Cu-K $_{\alpha 1}$ radiation (40 kV, 40 mA) over a 2θ range between 10° and 100° ($0.02^\circ/\text{step}$ with 8 seconds/step). The powder XRD pattern was compared with data from ICSD (Inorganic Crystal Structure Database, FIZ Karlsruhe and NIST) International diffraction database (ICSD#162758). [25] The structure was refined using the DBWS9807 free software. [26, 27]

The Raman spectra of the samples were acquired at room temperature in an iHR550 Horiba scientific spectrometer coupled to an Olympus microscope model BX-41. A He-Ne laser (632.8 nm, 10 mW) was used to excite the spectra that were collected in an air-cooled Synapse CCD detector. The spectral resolution was kept lower than 2 cm^{-1} using an 1800 grooves/mm grating in the spectrometer. All spectra were acquired in a backscattered configuration.

3. Computational method details

The first-principle calculations were performed through the Cambridge Serial Total Energy Package (CASTEP) software package [28]. Density functional theory (DFT) [29, 30] was chosen to model the material considering generalized gradient approximation (GGA) as exchange-correlation functional. This approximation was improved by the Perdew-Burke-Ernzerhof (PBE) parameterization [31]. The PBE functional leads to results close to those obtained using PW91 functional [32] within TS method [33] for the dispersion correction scheme (DFT+D) to describe van der Waals interactions. We also adopted pseudopotentials to replace the core electrons in each atomic species. Specifically, norm-conserved pseudopotentials [34] were used. These pseudopotentials were generated using the OPIUM code [35], following the same scheme of previous works [36, 37, 38]. The electronic valence configurations for each atomic species were: Ba- $5s^25p^66s^2$, Ca- $3s^23p^64s^2$, Nb- $4d^45s^1$, and O- $2s^22p^4$. A Monkhorst-Pack [39] $3 \times 3 \times 2$ sampling was used to evaluate all integrals in the reciprocal space. This sampling is enough to give a well converged electronic structure.

We employed BFGS minimizer [40] to optimize the unit cell. In this minimization algorithm, a starting Hessian is recursively updated. For each self-consistent field step, the electronic minimization parameters were: Total energy/atom convergence tolerance of 0.5×10^{-6} eV, a maximum energy eigenvalues threshold of 0.1442×10^{-6} eV, and a convergence window of 3 cycles. A plane-wave basis set was adopted to represent the Kohn-Sham orbitals, with cutoff energy chosen of 880 eV. This value was obtained after

convergence studies. The quality of this basis set was kept fixed as the unit cell volume varies during geometry optimization.

The vibrational properties of BCN were calculated performing density functional perturbation theory (DFPT) calculations or linear response formalism [41]. The linear response provides an analytical way of computing the second derivative of the total energy with respect to a given perturbation. Depending on the nature of this perturbation, a number of properties can be calculated. A perturbation in ionic positions gives the dynamical matrix and phonons; in the presence of magnetic field it gives the NMR response; in unit cell vectors changes it gives the elastic constants; in an electric field presence it gives the dielectric response, etc. The infrared absorption intensities are described in terms of a dynamical matrix and Born effective charges (also known as atomic polarizability tensors, ATP) [41] and can be obtained by calculating the phonons at the Γ point ($\vec{k} = 0$). The structure used for vibrational calculations was the fully ordered trigonal BCN structure optimized through the GGA-PBE approximation. The geometry optimization criteria were more rigorous than the criteria used for LDA-DFT calculations, for example. The convergence thresholds used were: Total energy convergence tolerance smaller than 5×10^{-6} eV/atom, maximum ionic force smaller than 10^{-2} eV/Å, maximum ionic displacement tolerance of 5×10^{-4} Å, and maximum stress component smaller than 2×10^{-2} GPa. For the self-consistent field calculations, the convergence criteria considered a total energy per atom variation smaller than 5×10^{-7} eV, and electronic energy eigenvalue variation smaller than 0.1442×10^{-6} eV.

4. Results and discussion

Figure 1 shows the powder X-ray diffraction pattern obtained for the *start sample*, which was sintered at 1300°C for 2h. The reflection planes were indexed according to the trigonal structure which belongs to the space group $P\bar{3}m1$. The refinement parameters were summarized in Table 1. In this structure the cations Ca^{2+} and Nb^{5+} are alternately distributed in $\{111\}$ planes in the form $\cdots \text{Ca} - \text{Nb} - \text{Nb} - \text{Ca} - \text{Nb} - \text{Nb} \cdots$. This distribution produces characteristic reflections of the trigonal superstructure.[42] When Ca and Nb are randomly distributed, and consequently the structure is disordered, the powder pattern does not exhibit such reflections, inducing changes in the plane indexing. In this case, a cubic structure that belongs to the space group $Pm\bar{3}m$ is usually observed.

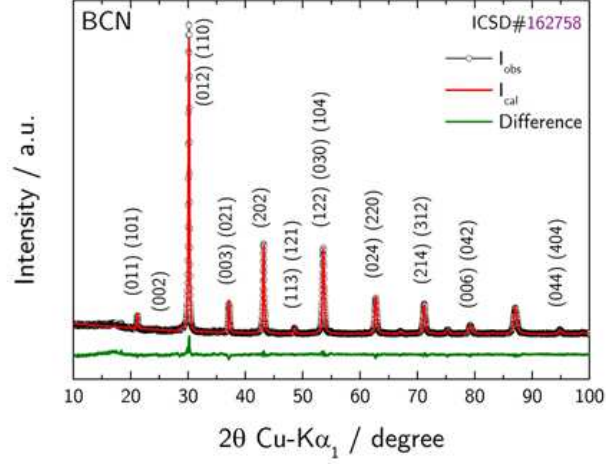


Figure 1: Powder X-ray diffraction pattern of BCN ceramic sintered for 1300 °C /2h. The solid line is the fitting using the Rietveld method and difference between the experimental and calculated patterns. The indices of planes are labeled in picture.

Space group; Z	$P3m1$ (N° 164); 3
Lattice parameters, Å	a=5.8921(8), c=7.2358(8)
Temperature, K	298(1)
Density (calculated), g/cm ³	5.965
Volume, Å ³	217.56
λ , Å	1.54056
Profile function	Pseudo-Voigt
Caglioti parameters (U, V, W)	0.2056(2), -0.0496(8), 0.0549(6)
Background function	5th order polynomial in 2θ
Rp, Rwp, Rexp, %	7.63, 10.05, 5.90

Table 1: Data collection and Refinement Details for BCN sample sintered for 1300°C for 2h.

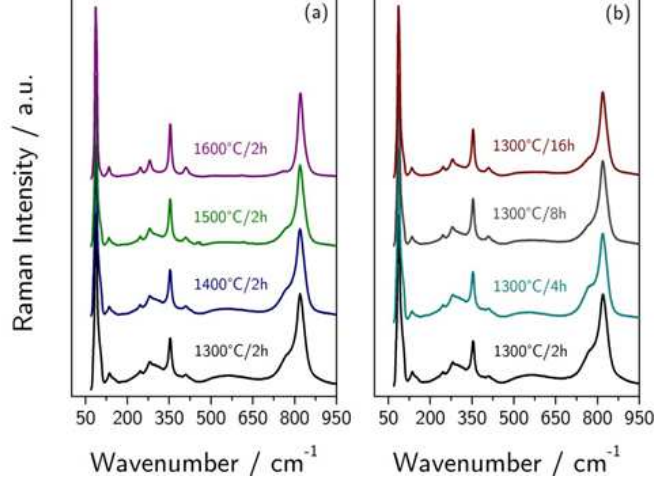


Figure 2: Raman spectra of the BCN ceramics sintered for several values of sintering temperature and sintering time.

To investigate the formation of ordered BCN structure we performed Raman scattering measurements in BCN samples sintered for several values of sintering temperature and sintering time. The observed Raman spectra are shown in Figure 2. To classify and identify the phonons observed we used a group theoretical analysis. Thus, we determined the symmetry and number of phonons in the full ordered trigonal structure based on the irreducible representation of the group factor $m\bar{3}m$. [43] In this structure the primitive unit cell has 15 atoms, where one barium ion is at the $1a$ site and two others are at the $2d$ site, the calcium ion is at $1b$ site and the two niobium ions are at $2d$ site, six oxygen ions are at $6i$ site and three are at the $3e$ site.[25, 44] Therefore, based on this ion occupation, the expected phonons in BCN are shown in Table 2. However, nine Raman-active modes ($4A_{1g} \oplus 5E_g$) are expected in BCN at room temperature.

In another way, occupational disorder can occur in two different ways: It implies in extra optical-active modes due to the different sites occupied by the ions (two-phonon behavior),[45] or it implies in local symmetry lowering (one phonon behavior),[46] changing the Raman and infrared spectrum. In this work we assumed the first case, that is the most common in 1:2 perovskites.[47, 45] Thus, to index the BCN crystalline structure according to the trigonal structure implies in an order-disorder model in which the trig-

Ion	Site	Symmetry	Distribution of modes
Ba1	1a	-3m	$A_{2u} \oplus E_u$
Ba2	2d	3m	$A_{1g} \oplus A_{2u} \oplus E_g \oplus E_u$
Ca1	1b	-3m	$A_{2u} \oplus E_u \oplus$
Nb1	2d	3m	$A_{1g} \oplus A_{2u} \oplus E_g \oplus E_u$
O1	3e	2/m	$A_{1u} \oplus 2A_{2u} \oplus 3E_u$
O2	6i	m	$2A_{1g} \oplus A_{1u} \oplus A_{2g} \oplus 6A_{2u} \oplus 3E_g \oplus 3E_u$
		Γ	$4A_{1g} \oplus 2A_{1u} \oplus A_{2g} \oplus 8A_{2u} \oplus 5E_g \oplus 10E_u$
		$\Gamma^{Acoustic}$	$A_{2u} \oplus E_u$
		Γ^{Raman}	$4A_{1g} \oplus 5E_g$
		Γ^{IR}	$7A_{2u} \oplus 9E_u$
		Γ^{Silent}	$2A_{1u} \oplus A_{2g}$

Table 2: Distribution of modes in the perovskite crystalline structure belonging to the trigonal space group $P\bar{3}m1$.

Ion	Site	Symmetry	Distribution of modes
Ca2	2d	3m	$A_{1g} \oplus A_{2u} \oplus E_g \oplus E_u$
Nb2	1b	-3m	$A_{2u} \oplus E_u$

Table 3: Distribution of modes for additional sites in the order-disorder model for the 1:2 perovskite compounds partially ordered.

onal perovskite structure is not fully ordered, although it still has a trigonal unit cell.[48, 47, 14, 49] In this case, there are part of calcium ion occupying the site 2d and part of niobium ion at the site 1b.[50, 51] Thus, in this order-disorder model, the group theoretical analysis can be used to predict the extra optical-active phonons based on extra site occupation by Ca and Nb ions, as showed in Table 3. Therefore, considering the disorder, there are now eleven Raman-active phonons in the partially ordered BCN.

From the Figure 2 (See bottom spectra in Figures 2(a) and 2(b)) we observed fourteen vibrational modes in the start sample, confirming a partially ordered 1:2 perovskite structure [47, 45] (see Figure 2b). Clearly, BCN Raman spectra change significantly when the sintering temperature and time are increased with both playing an essential role in ordering process.

The most ordered sample is achieved when sintered at 1600 °C for 2h, whose spectral deconvolution is shown in Figure 4 and summarized in Table 4.

To identify the Raman-active phonons in BCN and check the partial disordered model, we performed *ab initio* calculations of the vibrational properties of the full ordered BCN trigonal structure. The good reliability of the method employed can be seen comparing the experimental[25] and calculated structural data given in Table 5. The calculated phonons are summarized in Table 4 together with the experimental phonons. The infrared-active phonons are also shown for completeness.

The occurrence of the peaks n° 10 and 12 is correlated to the partial ordering adopted by the BCN confirming the disorder model adopted. This behavior can be explained by the Nb-O bond length decreases as consequence the Nb⁵⁺ substitution by the Ca²⁺, resulting in a displacement of the A_{1g} (821 cm⁻¹) mode to lower wavenumber.[44] Also, a simple harmonic model to these vibrations, based on the charge/mass relation $\frac{[q_{Ca}/m_{Ca}]^{1/2}}{[q_{Nb}/m_{Nb}]^{1/2}}$ give us the value 0.96, showing that the A_{1g} mode due to the extra-site Ca²⁺ occupation should be observed 0.96 times that A_{1g} band associate to the Nb⁵⁺ correct

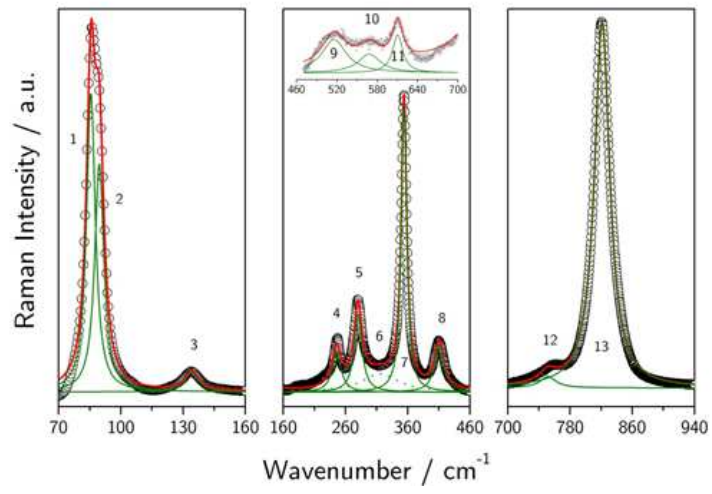


Figure 3: Deconvolution of the Raman spectra of the BCN pellet sintered at 1600°C / 2h. Collected data (o) and calculated Lorentzian (-) curve by fitting.

Table 4: Raman- and IR-active modes of trigonal BCN structure with respective attribution. A comparison between experimental (EXP.) and calculated (CAL.) data is shown to Raman modes. ^aFLB: Floating Base Line; ^bDAM: Defect activated IR-active modes.

Peak	Raman-active modes			Infrared-active modes	
	Center (EXP.)/cm ⁻¹	Center (CAL.)/cm ⁻¹	Attrib.	Center (CAL.)/cm ⁻¹	Attrib.
1	85.6	59.4	E_g	58.9	A_{2u}
2	89.6	60.4	A_{1g}	77.5	E_u
3	134.2	62.0	E_g	85.9	A_{2u}
4	245.6	241.2	A_{1g}	101.4	E_u
5	280.1	250.7	E_g	136.9	E_u
6	315.4	-	FLB ^a	179.6	E_u
7	353.9	305.8	E_g	191.8	E_u
8	410.5	356.8	A_{1g}	223.1	A_{2u}
9	515.9	-	DAM ^b	283.7	E_u
10	568.4	-	E_g	291.2	A_{2u}
11	610.5	658.9		352.4	E_u
12	751.5	-	A_{1g}	374.9	A_{2u}
13	821.2	827.7		503.7	E_u
		584.5	A_{2u}		
		663.1	E_u		
		807.8	A_{2u}		

occupation. [47] The calculated ratios, between the peaks n° 12 and 13 (0.92) and n° 10 and 11 (0.93) (see Table 4), show this assumption is correct.

The evaluation of the ordering kinetics of the BCN structure was followed according the evolution of the A_{1g} modes under the sintering temperature and time changes. A detailed spectral deconvolution of these modes are shown in Figure 4.

Clearly, the intensities of the peak n° 10 and 12 are proportional to the percentage of the extra-site Ca^{2+} and Nb^{5+} ions. Using the modes n° 12 and 13 we can estimate the ordering degree setting a ratio designated $\Psi_{Ca,Nb}$ expressed by

$$\Psi_{Ca,Nb} = \frac{I_{12,13}}{I_{12} + I_{13}} \quad (1)$$

When Ψ_{Nb} is equal to one, all Nb ions are in correct site. In this case Ψ_{Ca} is null. Thus, the fully ordered BCN structure occurs when $\Psi_{Ca} = I_{12} = 0$ and $\Psi_{Nb} = I_{13} = 1$. Figure 5 shows the evolution of the ratio $\Psi_{Ca,Nb}$ under the

a / Å	c / Å	γ	V / Å ³
GGA 6.0279	7.4631	120°	234.849
EXP. 5.9037	7.2636	120°	219.246

Table 5: Lattice parameters for BCN compound calculated within GGA-PBE calculation using the norm-conserving pseudopotential. Experimental data (EXP.) for BCN ceramic are also presented.[25]

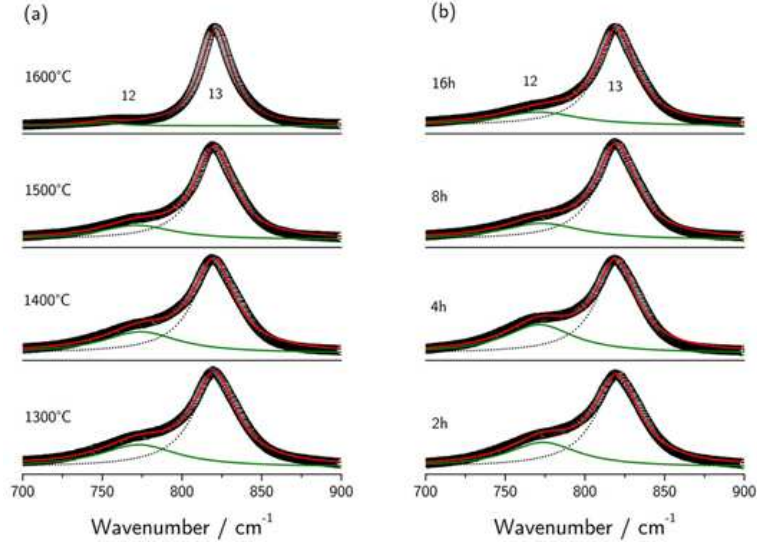


Figure 4: Deconvolution of the Raman spectra of the BCN ceramics in the spectral range 700-900 cm^{-1} for several values of sintering temperature (a) and sintering time (b). Collected data (o) and calculated Lorentzian (-) curve by fitting.

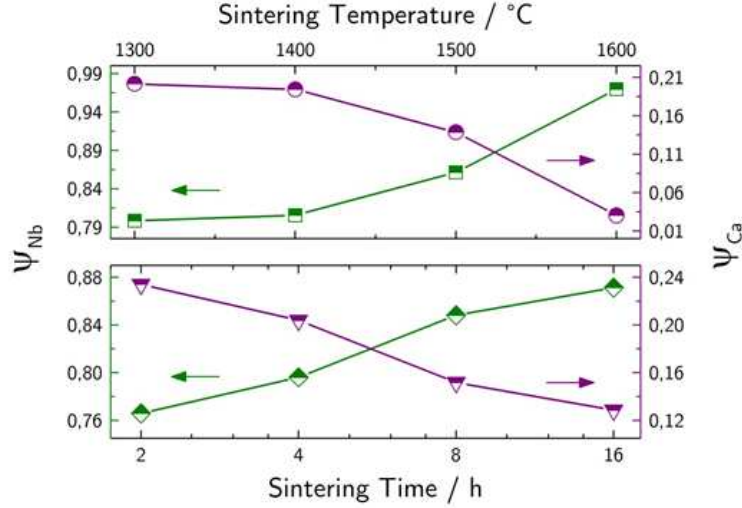


Figure 5: Behavior of the ratio $\Psi_{Ca,Nb}$ in function of the sintering temperature and of the sintering time for BCN ceramics.

sintering parameter changes. The most ordered sample is that sintered at 1600 °C for 2h for which Ψ_{Ca} (0.03) and Ψ_{Nb} (0.97). We observe the sintering time is not so efficient to order BCN, once that the calculated ratios to BCN ceramic sintered at 1300 °C for 16h were Ψ_{Ca} (0.13) and Ψ_{Nb} (0.87).

5. Conclusions

Partially ordered BCN ceramics was obtained by polymeric precursor method and the ordering in these samples were investigated by Raman spectroscopy under sintering temperature and sintering time changes. The evolution of the order was evaluated with basis on a partially ordered trigonal structure. An ab initio calculation permit us to assign the phonons and to monitor the order observing the changes in the behavior of the A_{1g} Raman-active mode near to 821 cm^{-1} . The most ordered sample was obtained at a sintering temperature of 1600 °C at 2 h.

Acknowledgement

The authors are grateful to the Brazilian funding agencies CAPES, CNPq, INCT NANOBIO SIMES and FAPEMA.

References

- [1] E. Ruiz-Trejo, R. A. D. Souza, R. a. De Souza, [Dopant substitution and oxygen migration in the complex perovskite oxide Ba₃CaNb₂O₉: A computational study](#), Journal of Solid State Chemistry 178 (6) (2005) 1959–1967.
- [2] A. Nowick, Y. Du, K. Liang, [Some factors that determine proton conductivity in nonstoichiometric complex perovskites](#), Solid State Ionics 125 (1-4) (1999) 303–311.
- [3] O. Valdez-Ramírez, F. Gómez-García, M. a. Camacho-López, E. Ruiz-Trejo, [Influence of the calcium excess in the structural and spectroscopic properties of the complex perovskite Ba₃CaNb₂O₉](#), Journal of Electroceramics 28 (4) (2012) 226–232.
- [4] S. S. Bhella, V. Thangadurai, [Investigations on the thermo-chemical stability and electrical conductivity of K-doped Ba₃xKxCaNb₂O₉δ \(x=0.5, 0.75, 1, 1.25\)](#), Solid State Ionics 192 (1) (2011) 234–229.
- [5] K. Oikawa, T. Kamiyama, S. Ikeda, T. Shishido, S. Yamaguchi, [Neutron powder diffraction studies on Ba₃Ca_{1+x}Nb_{2x}O₉_{3x/2} complex perovskite-type oxides](#), Solid State Ionics 154–155 (null) (2002) 641–646.
URL [http://dx.doi.org/10.1016/S0167-2738\(02\)00511-8](http://dx.doi.org/10.1016/S0167-2738(02)00511-8)
- [6] T. T. Trinh, V. Thangadurai, [Effect of Ti substitution for Nb in double perovskite-type Ba₃CaNb₂O₉ on chemical stability and electrical conductivity](#), Electrochimica Acta 56 (1) (2010) 227–234.
- [7] R. Mani, P. Selvamani, J. E. Joy, J. Gopalakrishnan, T. K. Mandal, [Study of Ba₃M\(II\)M\(IV\)WO₉ \(M\(II\) = Ca, Zn; M\(IV\) = Ti, Zr\) perovskite oxides: competition between 3C and 6H perovskite structures.](#), Inorganic chemistry 46 (16) (2007) 6661–7.
- [8] A. S. Bhalla, R. Guo, R. Roy, [The perovskite structure - a review of its role in ceramic science and technology](#), Materials Research Innovations 4 (1) (2000) 3–26.
- [9] A. Dias, C. W. A. Paschoal, R. L. Moreira, [Infrared Spectroscopic Investigations in Ordered Barium Magnesium Niobate Ceramics](#), Journal of the American Ceramic Society 86 (11) (2003) 1985–1987.

- [10] D. A. Sagala, S. Koyasu, [Infrared Reflection of Ba\(Mg_{1/3}Ta_{2/3}\)O₃ Ceramics](#), Journal of the American Ceramic Society 76 (10) (1993) 2433–2436.
- [11] A. Dias, R. L. Moreira, [Far-infrared spectroscopy in ordered and disordered BaMg\[_{1/3}\]Nb\[_{2/3}\]O\[₃\] microwave ceramics](#), Journal of Applied Physics 94 (5) (2003) 3414.
- [12] M. Lufaso, E. Hopkins, S. M. Bell, A. Llobet, Crystal Chemistry and Microwave Dielectric Properties of Ba₃MNb_{2-x}Sb_xO₉ (M = Mg, Ni, Zn), Chemistry of Materials 17 (16) (2005) 4250–4255.
- [13] Z. Yue, F. Zhao, Y. Zhang, Z. Gui, L. Li, [Microwave dielectric properties of Ba\[\(Zn_{1-x}Cox\)_{1/3}Nb_{2/3}\]O₃ ceramics](#), Materials Letters 58 (12-13) (2004) 1830–1834.
- [14] M.-Y. Chen, C.-T. Chia, I.-N. Lin, L.-J. Lin, C.-W. Ahn, S. Nahm, [Microwave properties of Ba\(Mg_{1/3}Ta_{2/3}\)O₃, Ba\(Mg_{1/3}Nb_{2/3}\)O₃ and Ba\(Co_{1/3}Nb_{2/3}\)O₃ ceramics revealed by Raman scattering](#), Journal of the European Ceramic Society 26 (10-11) (2006) 1965–1968.
- [15] K.-D. Kreuer, [Proton Conductivity: Materials and Applications](#), Chemistry of Materials 8 (3) (1996) 610–641.
- [16] B. A. Boukamp, [Fuel cells: The amazing perovskite anode.](#), Nature materials 2 (5) (2003) 294–6.
- [17] K. Truong, J. Laverdière, M. Singh, S. Jandl, P. Fournier, [Impact of CoMn cation ordering on phonon anomalies in La₂CoMnO₆ double perovskites: Raman spectroscopy](#), Physical Review B 76 (13) (2007) 132413.
- [18] C.-T. Lee, Y.-C. Lin, C.-Y. Huang, C.-Y. Su, C.-L. Hu, [Cation Ordering and Dielectric Characteristics in Barium Zinc Niobate](#), Journal of the American Ceramic Society 90 (2) (2007) 483–489.
- [19] P. K. Davies, J. Tong, T. Negas, [Effect of Ordering-Induced Domain Boundaries on Low-Loss Ba\(Zn_{1/3}Ta_{2/3}\)O₃-BaZrO₃ Perovskite Microwave Dielectrics](#), Journal of the American Ceramic Society 80 (7) (2005) 1727–1740.

- [20] M. A. Akbas, P. K. Davies, [Ordering-Induced Microstructures and Microwave Dielectric Properties of the \$\text{Ba}\(\text{Mg}_{1/3}\text{Nb}_{2/3}\)\text{O}_3\$ - \$\text{BaZrO}_3\$ System](#), Journal of the American Ceramic Society 81 (3) (2005) 670–676.
- [21] I. Levin, J. Chan, R. Geyer, J. Maslar, T. Vanderah, [Cation Ordering Types and Dielectric Properties in the Complex Perovskite \$\text{Ca}\(\text{Ca}_{1/3}\text{Nb}_{2/3}\)\text{O}_3\$](#) , Journal of Solid State Chemistry 156 (1) (2001) 122–134.
- [22] Y. H. Kim, I. T., Kim, Ordering and Microwave Dielectric Properties of $\text{Ba}(\text{Ni}_{1/3}\text{Nb}_{2/3})\text{O}_3$ ceramics, Journal of Materials Research 12 (2) (1997) 518–525.
- [23] J. E. F. S. Rodrigues, D. M. Bezerra, A. P. Maciel, A. R. Paschoal, C. W. A. Paschoal, [Ba\(\$\text{Zn}_{1/3}\text{Nb}_{2/3}\$ \) \$\text{O}_3\$ thin films obtained by polymeric precursors method](#), arXiv (2013) arXiv:1212.2272.
- [24] M. P. Pechini, U.s. patent no. 3.330.697, U.S. Patent No. 3.330.697.
- [25] J. Deng, J. Chen, R. Yu, G. Liu, X. Xing, [Crystallographic and Raman spectroscopic studies of microwave dielectric ceramics \$\text{Ba}\(\text{Ca}_{1/3}\text{Nb}_{2/3}\)\text{O}_3\$](#) , Journal of Alloys and Compounds 472 (1-2) (2009) 502–506.
- [26] H. M. Rietveld, [Line profiles of neutron powder-diffraction peaks for structure refinement](#), Acta Crystallographica 22 (1) (1967) 151–152.
- [27] H. M. Rietveld, [A profile refinement method for nuclear and magnetic structures](#), Journal of Applied Crystallography 2 (2) (1969) 65–71.
- [28] M. D. Segall, P. J. D. Lindan, M. J. Probert, C. J. Pickard, P. J. Hasnip, S. J. Clark, M. C. Payne, [First-principles simulation: ideas, illustrations and the CASTEP code](#), Journal of Physics: Condensed Matter 14 (11) (2002) 2717–2744.
- [29] W. Kohn, L. J. Sham, [Self-Consistent Equations Including Exchange and Correlation Effects](#), Physical Review 140 (4A) (1965) A1133–A1138.
- [30] P. Hohenberg, [Inhomogeneous Electron Gas](#), Physical Review 136 (3B) (1964) B864–B871.

- [31] J. P. Perdew, K. Burke, M. Ernzerhof, [Generalized Gradient Approximation Made Simple](#), Physical Review Letters 77 (18) (1996) 3865–3868.
- [32] J. P. Perdew, K. A. Jackson, M. R. Pederson, D. J. Singh, C. Fiolhais, [Atoms, molecules, solids, and surfaces: Applications of the generalized gradient approximation for exchange and correlation](#), Physical Review B 46 (11) (1992) 6671–6687.
- [33] A. Tkatchenko, M. Scheffler, [Accurate Molecular Van Der Waals Interactions from Ground-State Electron Density and Free-Atom Reference Data](#), Physical Review Letters 102 (7) (2009) 6–9.
- [34] J. Lin, A. Qteish, M. Payne, V. Heine, [Optimized and transferable non-local separable ab initio pseudopotentials](#), Physical Review B 47 (8) (1993) 4174–4180.
- [35] A. Rappe, K. Rabe, E. Kaxiras, J. Joannopoulos, [Optimized pseudopotentials](#), Physical Review B 41 (2) (1990) 1227–1230.
- [36] E. Moreira, J. M. Henriques, D. L. Azevedo, E. W. S. Caetano, V. N. Freire, U. L. Fulco, E. L. Albuquerque, [Structural and optoelectronic properties, and infrared spectrum of cubic BaSnO₃ from first principles calculations](#), Journal of Applied Physics 112 (4) (2012) 043703.
- [37] E. Moreira, J. Henriques, D. Azevedo, E. Caetano, V. Freire, E. Albuquerque, [Structural, optoelectronic, infrared and Raman spectra of orthorhombic SrSnO₃ from DFT calculations](#), Journal of Solid State Chemistry 184 (4) (2011) 921–928.
- [38] E. Moreira, J. Henriques, D. Azevedo, E. Caetano, V. Freire, E. Albuquerque, [Structural and electronic properties of Sr_xBa_{1-x}SnO₃ from first principles calculations](#), Journal of Solid State Chemistry 187 (2012) 186–194.
- [39] H. J. Monkhorst, J. D. Pack, [Special points for Brillouin-zone integrations](#), Physical Review B 13 (12) (1976) 5188–5192.
URL <http://link.aps.org/doi/10.1103/PhysRevB.13.5188>
- [40] B. G. Pfrommer, M. Cote, S. G. Louie, M. L. Cohen, [Relaxation of Crystals with the Quasi-Newton Method](#), Journal of Computational Physics 131 (1) (1997) 233–240.

- [41] S. Baroni, S. de Gironcoli, A. Dal Corso, [Phonons and related crystal properties from density-functional perturbation theory](#), Reviews of Modern Physics 73 (2) (2001) 515–562.
- [42] L. Galasso, F., Barrante, J. R., Katz, Alkaline Earth-Tantalum-Oxygen Phases Including the Crystal Structure of an Ordered Perovskite Compound $\text{Ba}_3\text{SrTa}_2\text{O}_9$, Journal of the American Chemical Society 83 (13) (1961) 2830–2832.
- [43] D. L. Rousseau, R. P. Bauman, S. P. S. Porto, [Normal mode determination in crystals](#), Journal of Raman Spectroscopy 10 (1) (1981) 253–290.
- [44] J. Deng, J. Chen, R. Yu, G. Liu, X. Xing, S. Han, Y. Liu, D. Chen, L. He, [Neutron powder diffraction study and B-site ordering in microwave dielectric ceramics \$\text{Ba}\(\text{Ca}_{1/3}\text{Nb}_{2/3}\)\text{O}_3\$](#) , Solid State Sciences 11 (1) (2009) 170–175.
- [45] A. Dias, V. Ciminelli, F. Matinaga, R. Moreira, [Raman scattering and X-ray diffraction investigations on hydrothermal barium magnesium niobate ceramics](#), Journal of the European Ceramic Society 21 (15) (2001) 2739–2744.
- [46] A. Ayala, C. Paschoal, I. Guedes, W. Paraguassu, P. Freire, J. Mendes Filho, R. Moreira, J.-Y. Gesland, [Disorder-induced symmetry lowering in the \$\text{CsInMgF}_6\$ pyrochlore crystal](#), Physical Review B 66 (21) (2002) 214105.
- [47] R. L. Moreira, F. M. Matinaga, A. Dias, [Raman-spectroscopic evaluation of the long-range order in \$\text{Ba}\(\text{B}'_{1/3}\text{B}''_{2/3}\)\text{O}_3\$ ceramics](#), Applied Physics Letters 78 (4) (2001) 428.
- [48] C.-T. Chia, Y.-C. Chen, H.-F. Cheng, I.-N. Lin, [Correlation of microwave dielectric properties and normal vibration modes of \$x\text{Ba}\(\text{Mg}_{1/3}\text{Ta}_{2/3}\)\text{O}_3\(1-x\)\text{Ba}\(\text{Mg}_{1/3}\text{Nb}_{2/3}\)\text{O}_3\$ ceramics: I. Raman spectroscopy](#), Journal of Applied Physics 94 (5) (2003) 3360.
- [49] K. P. Surendran, M. T. Sebastian, P. Mohanan, R. L. Moreira, A. Dias, Effect of Nonstoichiometry on the Structure and Microwave, Chemistry of Materials 17 (1) (2005) 142–151.

- [50] A. Siny, I.G., Tao, R., Katiyar, R.S., Guo, R., Bhalla, Raman Spectroscopy of Mg-Ta Order-Disorder in $\text{BaMg}_{1/3}\text{Ta}_2/3\text{O}_3$, Journal of Physics and Chemistry of Solids 59 (2) (1998) 181–195.
- [51] I. G. Siny, R. S. Katiyar, A. S. Bhalla, [Cation arrangement in the complex perovskites and vibrational spectra](#), Journal of Raman Spectroscopy 29 (5) (1998) 385–390.